JOURNAL OF COMPUTATIONAL PHYSICS 36, 71–92 (1980)

Macroscopic and Microscopic Models for the Relativistic Beam-Plasma Instability: A Comparison

KLAUS ELSÄSSER AND WINFRIED MAASJOST

Ruhr-Universität Bochum, Theoretische Physik I, 4630 Bochum, West Germany

Received July 6, 1978; revised April 4, 1979

The relaxation of a relativistic electron beam is studied in one space dimension by two different codes: (a) by a hybrid code where the fluid equations for the background plasma are integrated according to the pseudospectral method, and the beam particle equations by the particle-in-cell method; (b) by a pure particle-in-cell code. Thermal energy remains small in both simulations, which indicates that the fluid description is adequate to study the interaction. Beyond that, a quantitative comparison of the results shows good agreement; code (a) is more accurate due to the lower noise level, but it is also more sensitive to numerical instabilities. Finally, we show that simpler models like the single-wave model and its derivatives are in conflict with the correct wave–particle dynamics.

1. INTRODUCTION

The numerical study of plasma behavior has proceeded mainly along two lines which look physically and technically rather dissimilar: The plasma is treated either as a fluid or as an assembly of particles of finite size. While both ways of viewing the physical situation lead to well-known advantages and shortcomings of the corresponding numerical codes, relatively little is known of the feasibility and accuracy of a combination of both methods. Fluid equations may well be integrated by a particle-in-cell (PIC) technique (Harlow [1], Marder [2], Morse *et al.* [3], Leboeuf *et al.* [4]), but here we are thinking of a hybrid code: the combination of an ordinary fluid code, to be used for nonresonant particles, with an ordinary PIC code (Morse [5]) for resonant particles. A similar code operating on a long time scale has already been used by Rathmann *et al.* [6], but the specific advantages and shortcomings of a hybrid code do not seem to have been explored systematically in comparison with an ordinary particle code. Basic questions refer to the parameter range where the fluid code operates in a numerically stable regime, and also to the accuracy and economy of a hybrid code, in comparison with a pure particle code. It is true that the distinction between resonant and nonresonant particles may become artificial during the course of time for particular runs, but the use of few "representative" particles in a fluid with

0021-9991/80/070071-22$02.00/0

a low noise level is generally attractive as long as the plasma state can be reproduced this way.

We calculate the linear phase and the saturation of the relativistic two-stream instability in one space dimension with immobile ions. Code (a) integrates the fluid equations for the background electrons in an Eulerian manner (pseudospectral method) which can easily be used also in two and three space dimensions, while the beam electrons are treated individually according to the PIC technique. Code (b) integrates the equations of motion of all electrons individually according to the PIC method; it gives results similar to those obtained by Thode and Sudan [7] with a different numerical scheme.

In the next section we formulate the problem in more detail; Section 3 describes the numerical procedures; and Sections 4, 5, and 6 show the numerical results for the initial, linear, and saturated phases, respectively. Section 7 is devoted to the question of how the stability of the hybrid code can be improved, and how much time is saved or lost in comparable runs.

2. Formulation of the Problem

In case (a) we consider an electron fluid with mass density ρ and with the x-component of the velocity field

$$v = v^{\text{hom}} - \frac{\partial}{\partial x}\varphi,$$

where v^{hom} is the spatial average of v, over a periodicity interval of length L; and φ is the velocity potential. A relativistic electron beam moving in the x-direction excites an electric field

$$E = E^{\text{hom}} - \frac{\partial}{\partial x}\Phi,$$

where "hom" again means the spatial average, and Φ is the electric potential. Here the question arises whether the transverse modes play an essential role in more realistic two- or three-dimensional runs. At the present time this problem can only be discussed within the linear theory: for a beam propagating in an unmagnetized plasma, the growth rate of transverse modes is reduced both by small transverse velocities of beam particles and by increasing the temperature of the background plasma. The case of a beam propagating through a magnetized plasma along the magnetic field $\vec{B}$ is more subtle, but the growth rates have been computed by Godfrey *et al.* [8] with the following results: analytic expressions for the maximum growth rates of electrostatic modes in the "weak beam case" are in good agreement with those obtained from numerical solutions of the full electromagnetic dispersion relation, with the main exception that the numerical maximum growth rate of the two-stream instability for large $\vec{B}$ ($\omega_{ce} > \omega_{pe}$) drops off still faster with increasing angle between the wave vector and $\vec{B}$ than the analytical rate. Therefore, even the one-dimensional treatment seems to be adequate

in this case. Generally, we should use the following fluid equation for the velocity field of the background electrons:

$$\dot{\vec{v}} + (\vec{v} \cdot \nabla)\vec{v} + \nabla P = -\frac{e}{m}\left(\vec{E} + \frac{\vec{v}}{c} \times \vec{B}\right),$$

where the quantity

$$P = \int dp/\rho$$

is evaluated with adiabatic index 3. Equivalently we may write

$$\dot{\vec{v}} + \frac{e}{m}\vec{E}^{\text{hom}} + \nabla\left(\frac{v^2}{2} + P - \frac{e}{m}\Phi\right) = -\frac{e}{m}\vec{E}^{\text{tr}} + \vec{v} \times \vec{\Omega} \tag{1}$$

where $\vec{E}^{\text{tr}}$ is the transverse part of the electric field, and $\vec{\Omega}$ is the total vorticity:

$$\vec{\Omega} = \nabla \times \vec{v} - \frac{e}{mc}\vec{B}.$$

For *electrostatic* perturbations, we have $\vec{E}^{\text{tr}} = 0$, $\dot{\vec{B}} = 0$, and the generalized Helmholtz equation:

$$\dot{\vec{\Omega}} = \nabla \times (\vec{v} \times \vec{\Omega})$$

with the trivial solution $\vec{\Omega} = 0$ (corresponding to a rotation of the equilibrium plasma if $\vec{B} \neq 0$). The velocity field is then given according to the Clebsch representation [9] as

$$\vec{v} = \vec{v}^{\text{hom}} - \nabla\varphi + \chi\nabla\psi$$

with the time-independent vorticity

$$\nabla \times \vec{v} = (\nabla\chi) \times (\nabla\psi) = \frac{e}{mc}\vec{B}.$$

Equation (1) is then used to obtain the following two scalar equations:

$$\dot{\vec{v}}^{\text{hom}} = -\frac{e}{m}\vec{E}^{\text{hom}}, \tag{2a}$$

$$\dot{\varphi} = \frac{v^2}{2} + P - \frac{e}{m}\Phi. \tag{2b}$$

In the *one-dimensional case* we can put $\chi = \psi = 0$ without loss of generality and start immediately with Eq. (2a) and with Bernoulli's equation, Eq. (2b). The remaining set of equations then reads as follows:

$$\dot{\rho} = -\frac{\partial}{\partial x}(\rho v), \tag{3}$$

$$\dot{E}^{\text{hom}} = 4\pi \frac{e}{m}\{[\rho v]^{\text{hom}} + [\rho_b v_b]^{\text{hom}}\}, \tag{4}$$

$$\dot{x}_\mu = v_\mu , \tag{5}$$

$$\dot{u}_\mu = -\frac{e}{m} E, \tag{6}$$

$$\frac{\partial^2 \Phi}{\partial x^2} = 4\pi \frac{e}{m}(\rho + \rho_b - [\rho + \rho_b]^{\text{hom}}), \tag{7}$$

with

$$u_\mu = \gamma_\mu v_\mu ,$$
$$\gamma_\mu = (1 - v_\mu^2/c^2)^{-1/2},$$
$$\mu = 1, 2, \ldots, N_B .$$

Equation (3) expresses the mass conservation of the background electrons; Eq. (4) is the spatial average of Ampere's law; and ρ_b , v_b refer to the beam quantities which are obtained in an obvious manner from the (x_μ , v_μ) variables of each beam particle. Equations (5) and (6) are the relativistic equations of motion for the beam electrons. Finally, we have to solve Poisson's equation, (7), for every time step. At $t = 0$ we assume that the total current proportional to the right-hand side of Eq. (4) is zero, but for $t > 0$ this will not remain true. Therefore, we included the homogeneous variables E^{hom}, v^{hom}. The initial strength of the beam can be measured by the parameter S of Thode and Sudan [7]:

$$S = (v_b/c)^2 \gamma_b (\rho_b^{\text{hom}}/2\rho^{\text{hom}})^{1/3} \tag{8}$$

with

$$\gamma_b = (1 - v_b^2/c^2)^{-1/2}.$$

The beam energy is expected to be transformed partially into various other energies: electrostatic field energy, kinetic energy of background electrons, and thermal energy; but the total energy H should be invariant:

$$H = \int dx \left\{\frac{1}{8\pi} E^2 + \frac{1}{2}\rho v^2 + \int d\rho' \, P(\rho')\right\} + \sum_{\mu=1}^{N_B} m\gamma_\mu c^2; \tag{9}$$

the summation is over all beam particles. This will serve as a test for the numerical integration. Code (b) integrated only the particle equations (5) and (6) for both background and beam electrons simultaneously with (7).

The energy invariant now reads

$$H = \int dx \left\{\frac{1}{8\pi} E^2\right\} + \sum_{\mu=1}^{N} m\gamma_\mu c^2,$$

where N is equal to the total number of beam and background electrons.

3. Numerical Procedures

The system of Eqs. (2)–(7) has been integrated in dimensionless form by code (a); the corresponding figures in the following sections are also labeled by (a). The time integration has been done by a central explicit difference scheme of second order (leap frog). This is usual and well adapted for the PIC method [5], which has been used for treating the dynamics of the beam electrons and their contribution to the electric field (Eqs. (5), (6), and (7)). All x_μ are computed and used at integer time steps, all v_μ in between. But this leads to a difficulty in Eq. (4), where the mean beam velocity v_b is required at integer time steps; therefore, some interpolations or extrapolations are inevitable. The following closed system has been used for discretization in time:

$$(\alpha)\qquad \begin{aligned} u_\mu\left(t + \frac{\Delta t}{2}\right) &= u_\mu\left(t - \frac{\Delta t}{2}\right) + \Delta t\left(-\frac{e}{m}\right) E(t), \\ x_\mu(t + \Delta t) &= x_\mu(t) + \Delta t\, v_\mu\left(t + \frac{\Delta t}{2}\right); \end{aligned}$$

$$(\beta)\qquad \begin{aligned} \rho(t + \Delta t) &= \rho(t - \Delta t) + 2\Delta t\left(-\frac{\partial}{\partial x}\right)[\rho v](t), \\ \varphi(t + \Delta t) &= \varphi(t - \Delta t) + 2\Delta t\left[-\frac{e}{m}\Phi + \frac{1}{2}v^2 + P\right](t); \end{aligned}$$

$$(\gamma)\qquad \begin{aligned} E^{\text{hom}}\left(t + \frac{\Delta t}{2}\right) &= E^{\text{hom}}\left(t - \frac{\Delta t}{2}\right) + \Delta t\,\frac{4\pi}{c}\,\frac{e}{m}\{[\rho v]^{\text{hom}}(t) + [\rho_b v_b]^{\text{hom}}(t)\}, \\ v^{\text{hom}}(t + \Delta t) &= v^{\text{hom}}(t) + \Delta t\left(-\frac{e}{m}\right) E^{\text{hom}}\left(t + \frac{\Delta t}{2}\right). \end{aligned}$$

Assuming that all quantities are known at time t or $t - \Delta t/2$, respectively, we find the new particle coordinates according to (α) by converting $v_\mu(t - \Delta t/2)$ into $u_\mu(t - \Delta t/2)$ and reconverting $u_\mu(t + \Delta t/2)$ into $v_\mu(t + \Delta t/2)$. The fluid quantities ρ and φ are assumed to be known simultaneously at t and $t - \Delta t$; then we can advance them repeatedly according to (β). The homogeneous quantities are determined from (γ).

The value of v_b in a given cell of the x-space grid is obtained by computing the center-of-mass velocity of all particles contributing to the density in this cell. The mass assigned to a particle is determined by area weighting, and its velocity is taken to be the mean value of $v_\mu\,(t + \Delta t/2)$ and $v_\mu(t - \Delta t/2)$.

Finally, we have to mention that (α) requires the extrapolation of the homogeneous part of E from $t - \Delta t/2$ to t which has also been done linearly. The discretization in x has been replaced by truncating the Fourier series of ρ and φ, respectively; (β) and Poisson's equation have been solved in Fourier space. The convolution sums arising from the nonlinear terms have been evaluated in the fastest manner by transforming the factors into x-space and retransforming the product into Fourier space without removing the aliasing interactions. This pseudospectral method has been found to be less accurate for wave propagation problems than the spectral method (Schamel and Elsässer [10]), but in the present problem the accuracy was sufficient for the comparison between results (a) and (b). The starting values of ρ and φ in case (a) were obtained by simulating the thermal noise in Fourier space at $t = 0$ with a Monte Carlo method, and by distributing the beam particles uniformly in x-space with equal velocity v_b (cold beam). The second values of ρ and φ which are needed to start (β) were obtained with Euler's method. The general procedure for (a) is shown in the flow diagram.

Code (b) integrated only the particle Eqs (5) and (6) for both background and beam electrons simultaneously with (7) according to PIC; the initial distribution of background electrons was spatially homogeneous and Maxwellian in velocity space; its mean velocity v^{hom} has been chosen as in case (a) to cancel the initial beam current.

4. Initial Phase

The following initial parameters have been chosen ($v_{\text{the}} = (\kappa T_e/m_e)^{1/2}$ = thermal speed of background electrons; λ_D = Debye length = $v_{\text{the}}/\omega_{pe}$):

$$v_b/c = 0.9; \qquad v_{\text{the}}/c = 0.1.$$

Number of cells in k- or x-space:	128.
Maximum wave number ($= \pi/\Delta x$):	λ_D^{-1}.
$\rho_b^{\text{hom}}/\rho^{\text{hom}}$ in case (a):	0.05.
Number of beam electrons:	256 for (a), 768 for (b).
Number of background electrons for (b):	15,616.
Time step Δt in units of ω_{pe}^{-1}:	0.05 for (a), 0.5 for (b).

The resulting beam strength parameter (Eq. (8)) is $S = 0.4$ in both cases.

After some time steps, we observed the following mean values (in space and time) of the turbulence parameter:

$$\frac{\langle E^2 \rangle}{8\pi n_0 \kappa T_e} = 7.8 \times 10^{-6} \quad \text{for (a)},$$

$$= 2.3 \times 10^{-3} \quad \text{for (b)}.$$

In (a) we have chosen small initial Fourier amplitudes, thus producing a low noise level. Its order of magnitude corresponds to the thermal noise of real plasmas. The higher value, according to (b), is in rough agreement with the formula for the thermal noise of a 1 — d plasma with the parameters of code (b), namely:

$$\frac{1}{2\pi} \frac{1}{n_0 \lambda_D} = 4 \times 10^{-3}.$$

The observed lower value in case (b) is probably due to the finite size of the particles: for particles of length a with homogeneous charge density, one obtains the following shape factor for the charge density (Birdsall *et al.* [11]):

$$S(k) = \sin(ka)/(ka). \tag{10}$$

The Fourier transform of the density of point particles has to be multiplied by the square of this expression, leading thus to a decreasing electric field at high wave numbers k.

5. Linear Phase

The wave number of the most unstable mode is given according to the linear theory by

$$k_0 = \omega_{pe}/v_b \approx (2\pi/L)[k_0] \tag{11}$$

with

$$[k_0] = 7.$$

We have calculated the growth rates for this and the two neighboring modes 6 and 8 from the dispersion relations

$$1 = \frac{\omega_{pe}^2}{(\omega - kv^{\text{hom}})^2} + S^2(k) \frac{n_b \omega_{pe}^2}{n_0 \gamma_b^3 (\omega - kv_b)^2}, \tag{12a}$$

$$1 = S^2(k) \frac{\omega_{pe}^2}{(\omega - kv^{\text{hom}})^2} + S^2(k) \frac{n_b \omega_{pe}^2}{n_0 \gamma_b^3 (\omega - kv_b)^2}, \tag{12b}$$

$$1 = \frac{\omega_{pe}^2}{(\omega - kv^{\text{hom}})^2} + \frac{n_b \omega_{pe}^2}{n_0 \gamma_b^3 (\omega - kv_b)^2}, \tag{12c}$$

where $S(k)$ is the shape factor given by Eq. (10). Equations (12a) and (12b) are the approximate dispersion relations for the runs (a) and (b), respectively, when the temperature of the background electrons can be neglected. Equation (12c) is the corresponding relation for the case of point particles. The results for these "theoretical" growth rates are displayed in Table I. The effect of the shape factor is obviously more pronounced in case (b) than in (a). The observed growth rates in Table I are obtained from Fig. 1a and b, where the logarithm of the squared modulus of the electric field amplitude for the three modes is plotted as function of time. Both figures clearly show a linear phase; the corresponding slopes give twice the experimen-

TABLE I

Comparison of Growth Rates for the Three Most Unstable Modes

		(a)		(b)		(c)
$[k]$	$k\lambda_D$	Theor.	Exp.	Theor.	Exp.	Eq. (12c)
6	0.094	0.091	0.088	0.091	0.073	0.091
7	0.109	0.103	0.103	0.101	0.101	0.104
8	0.125	0.075	0.082	0.057	0.081	0.076

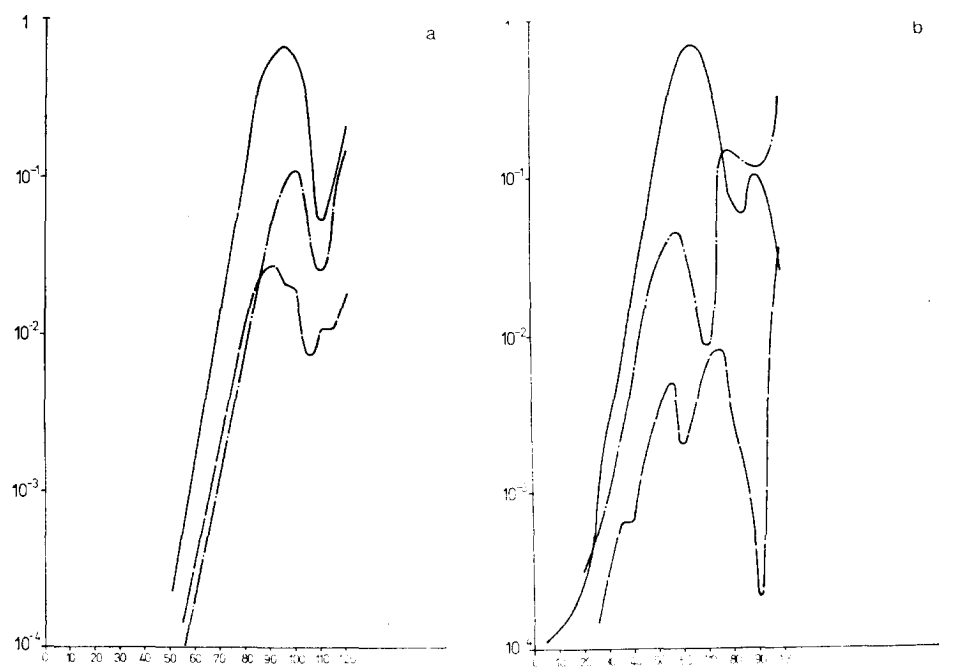

FIG. 1. Wave energy $|E_K|^2/8\pi(\rho + \rho_b)\kappa T_e/m$ for the three most unstable modes as a function of time.

tal growth rates of Table I in units of ω_{pe}. The general agreement between theoretical and experimental growth rates is satisfactory. Deviations are due to the finite cell size whose effect on the dispersion relation is not included in the PIC theory. In code (a), we have computed the evolution of Fourier modes, thus doing numerically what is done analytically in linear theory. Differences arise from the finite time step and the PIC technique used for the beam. Because its density is small, the results in code (a) are in better agreement with theory than those in (b), where PIC has been used for beam and plasma. The different noise level is responsible for the different time intervals where the linear phase can be observed. The times for (a) and (b) physically corresponding with each other can be obtained by comparing figures which show the same stage of the evolution, e.g., we can compare the phase space plots of the beam particles in Figs. 2a ($\omega_{pe}t = 80$) and 2b ($\omega_{pe}t = 50$), where the most unstable mode has reached a comparable fraction of its saturation level. We find essentially the same distribution functions up to a phase shift in x. The density contrast is better in Fig. 2b, since the number of beam particles in (b) is three times higher than in (a) (though the relative numbers are equal). The distribution of beam particles retraces the electric field in this phase. It is not sinusoidal due to the presence of the modes with k slightly different from k_0, and due to a modulation with the basic wave number $2\pi/L$.

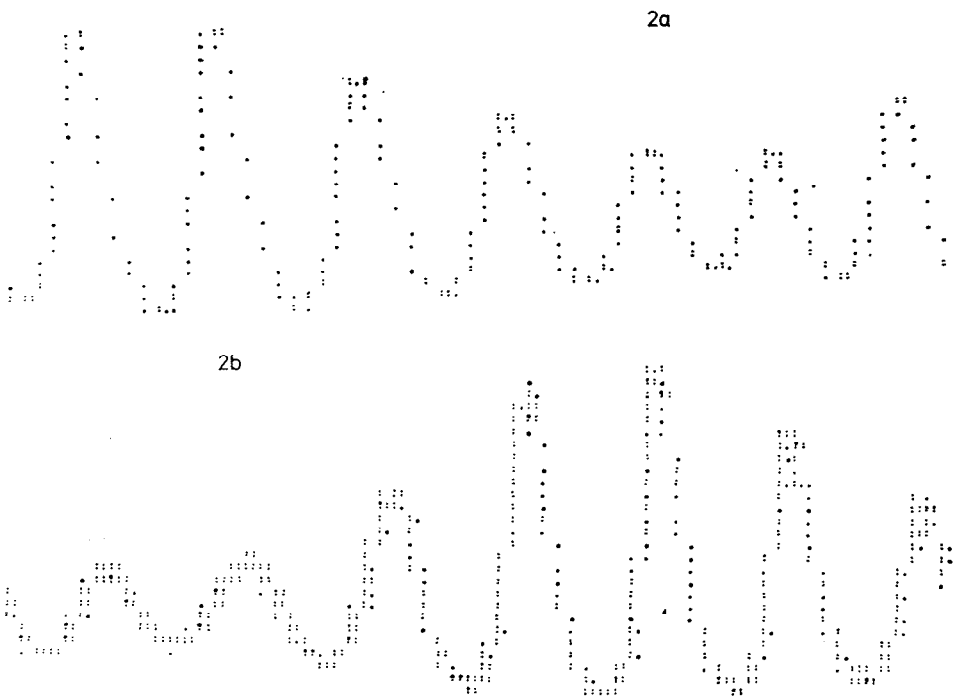

FIG. 2. Distribution of beam particles in phase space at $\omega_{pe}t = 80$ (a) and $\omega_{pe}t = 50$ (b). V and x are increasing from the top to the bottom and from the left to the right, respectively.

6. Saturated Phase

The linear phase is terminated if the beam particles become slow enough to be trapped in the moving potential waves. Shortly before trapping these particles are localized in x-space, and the higher harmonics of the most unstable modes are generated. Figures 3a and b depict the electric field energy density as a function of the

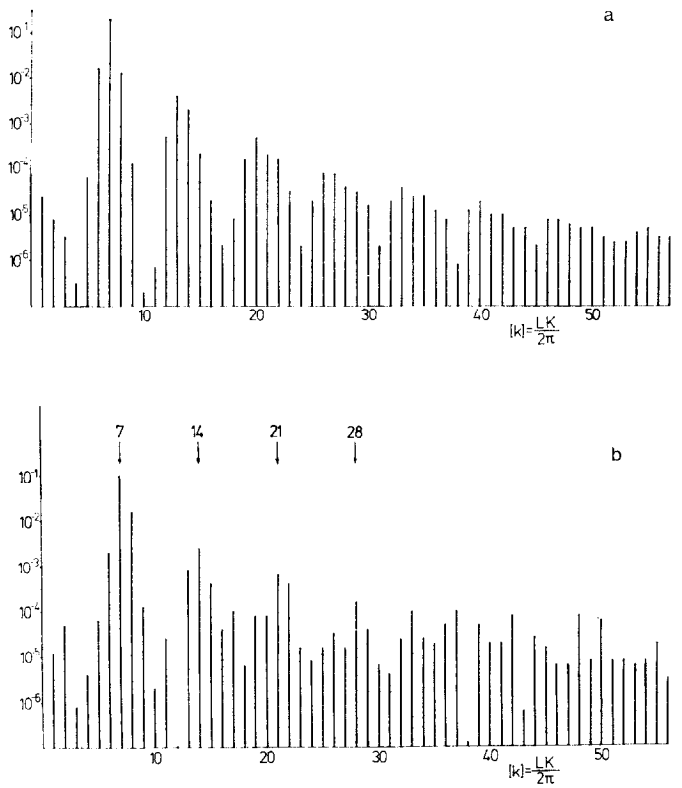

Fig. 3. Wave energy $|E_K|^2/8\pi(\rho + \rho_b)\kappa T_e/m$ as a function of wavenumber shortly before saturation.

wave number; in case (a) the generation of higher harmonics is more pronounced due to the lower noise level. In both cases the trapping could clearly be seen by inspection of the whirls in the phase space plots of the beam particles; after the saturation time t_s, where the field energy reaches a first maximum,

$$W = \sum_k |E_k|^2/8\pi n_{b0}\gamma_{b0}m_e c^2 = 0.074 \quad \text{for (a)},$$
$$= 0.072 \quad \text{for (b)}, \tag{13}$$

we observe a quasi-periodic energy exchange between the beam and background particles. Figures 4a and b show the time evolution of several energies listed in Eq. (9): beam energy (curve 1), total background energy (curve 2), and electric field energy (curve 3) in different units. The drop of the field energy from the first maximum at

$$\begin{aligned} \omega_{pe} t_s &= 96 \quad \text{for (a)}, \\ &= 66 \quad \text{for (b)}, \end{aligned} \tag{14}$$

to a minimum is more pronounced in (a) because the bunching of the beam particles in x-space is more effective in the fluid code. We find

$$\begin{aligned} \text{minimum of field energy} &= 15\% \text{ of maximum for (a)}, \\ &= 40\% \text{ of maximum for (b)}. \end{aligned}$$

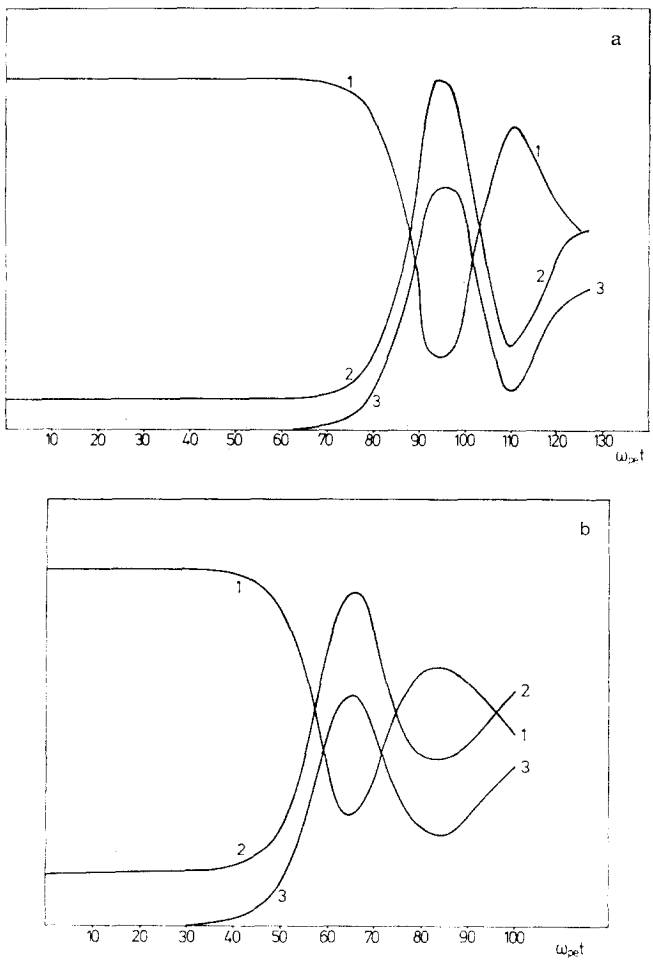

FIG. 4. Beam energy (1), plasma energy (2), and field energy (3) as functions of time (arbitrary units; curves labeled identically also have identical scales).

It is interesting to compare, also, the thermal part of the background energies because the adiabatic law in case (a) is, in general, physically different from an empirical law, which would match the results in case (b). We have calculated the mean velocity of the background particles in case (b) and subtracted the corresponding ordered kinetic energy from the total background energy; the remaining energy called thermal energy has been compared at the end of the run with the corresponding quantity at $t = 0$. We find

Increase of total background energy per particle, $\Delta E_{nr} = 1.07 \times 10^{-2} m_e c^2$ for (a)
$= 0.92 \times 10^{-2} m_e c^2$ for (b).
Increase of thermal energy per particle: $= 5.4\ \%$ of ΔE_{nr} for (a),
$= 10.2\ \%$ of ΔE_{nr} for (b).

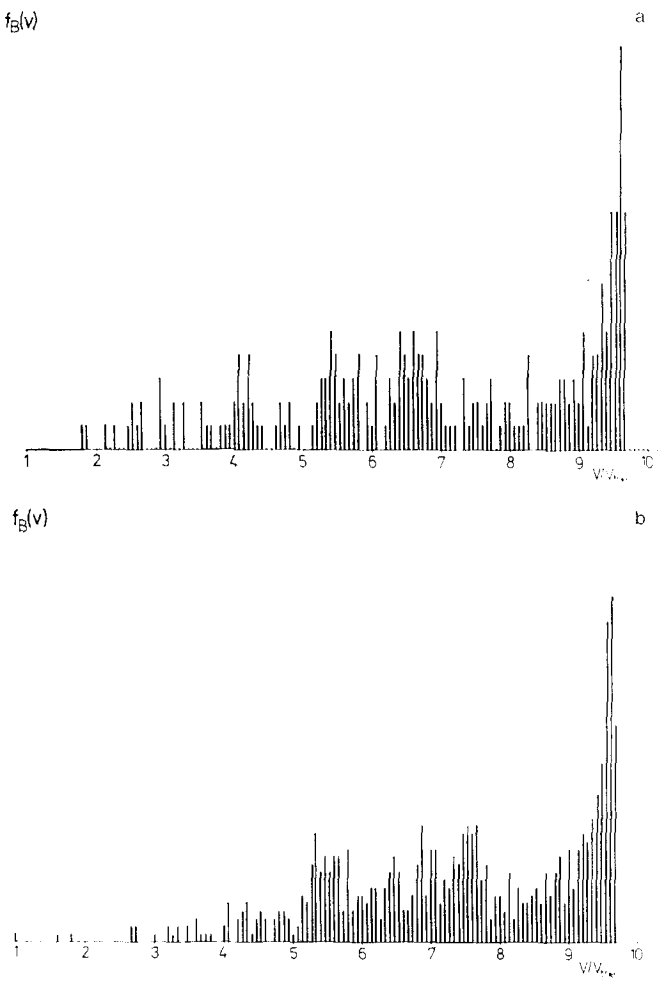

FIG. 5. Homogeneous beam distribution function at saturation. The step size for f_B is one particle per velocity interval in both cases, normalized to equal numbers of beam particles.

Therefore, the adiabatic law is not really consistent with the PIC simulation, but in both cases the thermal energy is only a small fraction of the total background energy and the difference can be ignored. The variation of the total energy H, according to Eq. (9), has also been measured:

$$\Delta H = 0.10\% \text{ of } H \text{ for (a)},$$
$$= 0.14\% \text{ of } H \text{ for (b)},$$

which is still an order of magnitude smaller than the increase of the thermal background energy.

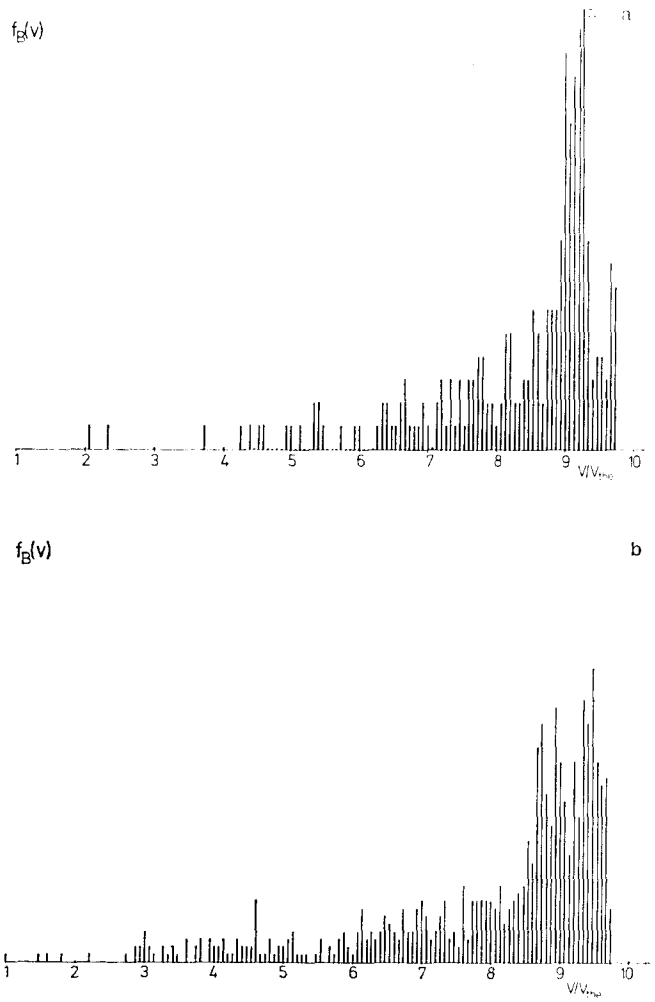

FIG. 6. Same as Fig. 5, but at the first minimum of the field energy.

The spatially averaged beam particle distribution function $f_B(v)$ has been observed at the times t_s, $t_{\min}$ of maximum and minimum field energy, respectively. At $t = t_s$ we find a high-energy part around $v \approx 0.96c = 9.6v_{the}$ and a relatively flat part for $v \lesssim 0.9c$ in Figs. 5a and b. Figures 5a and b have been normalized to equal beam particle numbers. Later on, the beam particles are accelerated by the waves, and we expect higher energies at $t = t_{\min}$. This is confirmed by Figs. 6a and b, where a group of particles has been moved from the flat part of the distribution function to higher velocities. We define a number N_H of high-energy particles

$$N_H = \int_{0.9c}^{c} dv\, f_B(v),$$

and find the following results:

$$N_H|_{t=t_s} = 28.5\,\% \text{ of } N_B \text{ for (a)},$$
$$= 28.8\,\% \text{ of } N_B \text{ for (b)}.$$

$$N_H|_{t=t_{min}} = 48.8\,\% \text{ of } N_B \text{ for (a)},$$
$$= 37.6\,\% \text{ of } N_B \text{ for (b)}.$$

Up to $t = t_s$ we see rather similar distribution functions, but for $t = t_{\min}$ the differences are more pronounced. The PIC code produces a smearing out of the particle phases at this time as compared with code (a). The same phenomenon could also be supposed when comparing the minima of background and field energies in Figs. 4a and b.

7. Stabilizing Procedures and Competitive Runs

An ideal code would combine the numerical stability of the PIC code, allowing large time steps, with the economy (per time step) and numerical accuracy of the fluid code. Of course, we have not achieved this goal, but some steps have been made in this direction. Here we present the results of several runs both for (a) and (b), where some time-saving and/or stabilizing procedures have been applied.

The time step in an explicit scheme is usually limited by the requirement of numerical stability of the modes with highest frequency $\omega_{\max}$. Using the linear fluid part of the equations of motion (β) and the fluid part of Poisson's equation (7) as a guide, we obtain the usual dispersion relation for Langmuir waves:

$$\omega_k^2 = \omega_{pe}^2(1 + 3k^2\lambda_D^2)$$

with the cut-off

$$k_{\max}\lambda_D = \frac{2\pi}{128\,\Delta x} \cdot 64 \cdot \lambda_D = 1$$

and, therefore,

$$\omega_{\max} = 2\omega_{pe},$$

a rather high value where Landau damping should be included. But the trapping phase has also been found to be critical for stability, requiring $\omega_{pe}\Delta t \ll \omega_{pe}/\omega_{\max} = 0.5$ and leading us to the extremely small value of $\omega_{pe}\,\Delta t = 0.05$. The situation gets still worse for a run with $\Delta x \approx \lambda_D$, $k_{\max}\lambda_D \approx \pi$, $\omega_{\max} \approx 5\omega_{pe}$.

Therefore, we explored two methods to improve the stability of the fluid code.

The first method is a semi-implicit time discretization scheme of second-order accuracy for the equations (β) of the form

$$\frac{1}{2\Delta t}\,[\mathbf{u}_{t+\Delta t} - \mathbf{u}_{t-\Delta t}] = \frac{1}{2}\,\mathbf{L}\cdot[\mathbf{u}_{t+\Delta t} + \mathbf{u}_{t-\Delta t}] + \mathbf{N}(\mathbf{u}_t, \mathbf{u}_t), \tag{15}$$

where the elements of the vector $\mathbf{u}_t$ are the unknown functions ρ, φ at time t:

$$\mathbf{u}_t = \begin{pmatrix}\rho(t, x)\\ \varphi(t, x)\end{pmatrix},$$

and the matrix L comprises the linear operators of the right-hand side of (β) acting on ρ, φ; the vector $\mathbf{N}(\mathbf{u}_t, \mathbf{u}_t)$ represents the remaining terms.

In Fourier space, we have

$$\mathbf{L} = \begin{pmatrix}0, & -\rho_0 k^2\\ \omega_k{}^2/\rho_0 k^2, & 0\end{pmatrix},$$

where Φ has been eliminated by the Poisson equation (7); $N(u_t, u_t)$ is a collection of convolution sums and also includes the potential of the beam particles. Solving Eq. (15) for the unknown vector $u_{t+\Delta t}$, we obtain the following scheme in Fourier space:

$$\mathbf{u}_{t+\Delta t} = \mathbf{A}\cdot\mathbf{u}_{t-\Delta t} + \mathbf{B}\cdot\mathbf{N}(u_t, u_t) \tag{16}$$

with

$$\begin{aligned}\mathbf{B} &= 2\Delta t(\mathbf{1} - \Delta t\,\mathbf{L})^{-1}\\ &= \frac{2\Delta t}{1 + (\omega_k\,\Delta t)^2}\,(\mathbf{1} + \Delta t\,\mathbf{L}),\\ \mathbf{A} &= \mathbf{1} + \mathbf{B}\cdot\mathbf{L}\\ &= \frac{1 - (\omega_k\,\Delta t)^2}{1 + (\omega_k\,\Delta t)^2}\,\mathbf{1} + \frac{2\Delta t}{1 + (\omega_k\,\Delta t)^2}\,\mathbf{L},\end{aligned}$$

where $\mathbf{1}$ is the unit matrix. A fully implicit scheme would be unconditionally stable, as is well known for ordinary differential equations (see, e.g., Potter [12]). The stability properties of scheme (16) will, therefore, depend only on the nonlinear and the beam

terms (as comprised in $\mathbf{N}(\mathbf{u}_t, \mathbf{u}_t)$) for which no simple implicit method seems to be available. Indeed, for $\mathbf{N}(\mathbf{u}_t, \mathbf{u}_t) \equiv 0$ we can easily show that Eq. (16) produces the following solution for the Fourier modes:

$$\mathbf{u}_t \sim \exp(-i\omega t)$$

with

$$\begin{aligned} \mathrm{Im}(\omega) &= 0, \\ \sin(2\omega\,\Delta t) &= 2\omega_k\,\Delta t/[1 + (\omega_k\,\Delta t)^2] \\ &\leqslant 1 \qquad \text{for any positive value of } \omega_k\,\Delta t. \end{aligned}$$

But for runs with $\Delta x \approx \lambda_D$, a second method is needed for stabilizing the code during the trapping phase. In calculating the electrostatic potential from Poisson's equation, we have truncated the number density of the beam particles in Fourier space for $|k| \geqslant \frac{3}{4} k_{\max}$ (instead of $|k| \geqslant k_{\max}$); the effect of this operation—in the following we call it "beam truncation"—is similar to an increase of the size of the beam particles with fixed cell size Δx for the fluid code. In order to have a fair comparison, we also produced several runs with code (b) by varying the total particle number, the time step, cell size, and also by splitting each of the beam particles into 10 particles of the weight 1/10 with respect to charge and mass. This operation, called "beam splitting" in the following, is equivalent to reducing the number of the background particles whose weight increases correspondingly (Kainer *et al.* [13]). The relevant parameters for several runs are listed in Table II; runs 1(a) and 1(b) have been shown previously. N_B is the number of actually calculated beam particles, N the total number of actually calculated particles in case (b). The CPU time as measured on an IBM 370-168 computer fluctuates by about 10% according to the actual time sharing in connection with other users. It has been extrapolated to 2000 time steps in each case, though most of the particle runs (b) needed only 200 steps. Runs 4(a), 4(b) have been designed with equal time step, space grid, and number of beam particles, and should, therefore, be compared with respect to computer time and accuracy. Instead of showing all figures again we can limit ourselves to the time evolution of the most unstable mode, which is a rather sensitive tool for illustrating the effect of parameter changes. Figure 7a shows the results of the hybrid code. Run 2(a) could not be continued due to numerical instability; therefore, runs 3(a) and 4(a) used the semi-implicit scheme according to Eq. (16). While a change in Δx still gives significant effects, we observe readily that neither a change in Δt nor the beam splitting of run 4(a) gives remarkable modifications of the standard run 1(a). Figure 7b of the particle code shows that a decrease of Δx as well as the other changes lead to a more pronounced spread of the data. The earlier rise time of the mode for runs 2(b)–5(b) is due to the higher noise level, which is mainly determined by the background particles. In view of this material, we can say that the hybrid code is, for similar parameters, faster and more accurate than the particle code; but its stability remains a problem for runs with high spatial resolution or with long evolution times.

TABLE II

Characteristic Parameters for Several Runs.

Run	$\omega_{pe}\Delta t$	$\Delta x/\lambda_D$	Beam splitting	Beam truncation	N_B	CPU time for 2000 time steps (min)	N	Symbol in Fig. 7
1(a)	0.05	π	no	no	256	14,5		×
2(a)	0.05	0.9	no	no	256	13,5		○
3(a)	0.05	0.9	no	yes	256	14,5		△
4(a)	0.1	π	yes	no	2,560	32,0		▽
1(b)	0.5	π	no	no	768	108,5	16,384	×
2(b)	0.5	π	yes	no	2,560	52,5	7,936	▽
3(b)	0.5	0.9	yes	no	2,560	54,0	7,936	△
4(b)	0.1	π	yes	no	2,560	48,0	7,936	⊙
5(b)	0.5	π	no	no	256	42,0	5,632	□

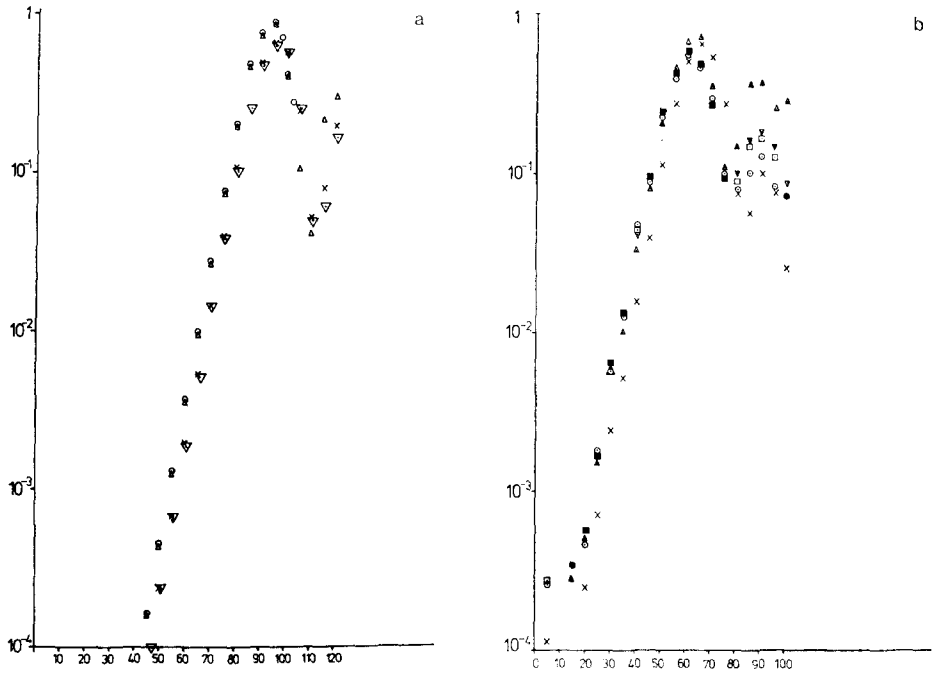

FIG. 7. Time evolution of the wave energy of the most unstable mode for several runs as listed in Table II. ■: coincidence of □ and ▽; ●: coincidence of ⊡ and ⊙.

8. SUMMARY AND DISCUSSION

We have calculated the relaxation of a relativistic electron beam in an electron plasma with fixed ions in one space dimension, using two different numerical schemes. Code (a) integrated the fluid equations for the background electrons simultaneously with the beam particle equations and Poisson's equation, while code (b) was a pure simulation code according to the particle-in-cell technique. All features of the relaxation process, such as linear growth, particle trapping, generation of high-energy particles, and oscillations of beam and background energies, are better seen in code (a), due to the fact that the initial noise level could be chosen freely in accordance with the noise of a real plasma, while the noise in code (b) results from the restricted number of background electrons and is, therefore, notoriously high. One of the best agreements between the results of (a) and (b) in the nonlinear phase was the first maximum of the field energy, Eq. (13). Thode and Sudan [7] give the following formula for this quantity:

$$W_{TS} = \tfrac{1}{2}S(1 + S)^{-5/2},$$

where S is the initial beam strength parameter as defined in Eq. (8). In our runs we have to put $S = 0.4$ and obtain

$$W_{TS} = 0.087,$$

a value which is almost 20% too high. But this difference reflects only the inaccuracy of the formula for W_{TS}. In a run similar to ours with $\gamma_b = 2$; $n_{b0}/n_{e0} = 0.05$; $L/\lambda_D = 710$, the same authors obtained a saturation energy which is 4% lower than ours. The difference of the saturation times t_s according to Eq. (14) can be explained by the different initial noise levels for (a) and (b). Extrapolating the exponential growth of $W(t)$ from $t = 0$ to $t = t_s$, we obtain the following estimate:

$$\exp(2\gamma_0 t_s) \approx W(t_s)/W(0).$$

Using the growth rate γ_0 of the most unstable mode according to Table I and the values for the initial noises as given in Section 4, we obtain for the difference Δt_s of t_s between (a) and (b)

$$\omega_{pe}\,\Delta t_s \approx \frac{1}{2 \times 0.10} \ln \frac{2.3 \times 10^{-3}}{7.8 \times 10^{-6}} = 28,$$

which is in good agreement with the observed value 30 because the true values of $W(t_s)$ are nearly equal and cancel each other. Thus, it seems that the fluid code is optimally adapted for calculations in two and three space dimensions for cold and warm beams since the storage requirements are considerably lower than for the PIC code. But we also have to mention two disadvantages which are implied by the high accuracy of the present code (a): first, it required a time step which was only one-tenth of the step in (b), and second, the generation of higher harmonics of the electric field, due to the bouncing motion of the trapped beam particles, is dangerous for the numerical stability of code (a). We have not yet found a sufficiently stable and dissipationless scheme which would also allow the calculation of the parametric phase where the stabilized beam modes drive the ion fluctuations unstable. Finally, we want to discuss our results with respect to further simplifications of the fluid description. O'Neil *et al.* [14] and Matsiborko *et al.* [15] reduced the fluid description of the background to the equation for the most unstable mode interacting with the beam particles; later on this single wave model was extended by Schamel *et al.* [16] to study the parametric phase. A common feature of these approaches is the appearance of an invariant of motion, the generalized plasmon number, which restricts the redistribution of beam energy. In the absence of a beam, this invariance follows from a time scale argument even if many waves (Langmuir and ion sound) are present, as was shown by Elsässer and Schamel [17]. In the presence of a cold beam, the same argument leads to a new invariant, provided that the spectrum of the high-frequency waves is sufficiently narrow; one finds the following generalized plasmon number (Maasjost [18]):

$$PN = N_P + (n_{b0}/k_0)\langle p \rangle, \tag{17}$$

where N_P is the ordinary plasmon number and $\langle p \rangle$ the mean momentum of the beam particles. We observed the field energy W_0 of the mode k_0 at saturation time t_s and we found

$$W_0 = 80.5\% \text{ of } W \text{ for (a)},$$
$$= 88.0\% \text{ of } W \text{ for (b)},$$

a result which seems to be in favor of the single-wave model. But we also observed the time evolution of PN in code (a) as shown in Fig. 8: it is not at all constant. The sloshing motion of the trapped particles is in conflict with the assumption of separated time scales even if the spectrum is narrow. Therefore, the fluid description involving many modes seems to be the simplest physical model which gives the correct dynamics of the background plasma.

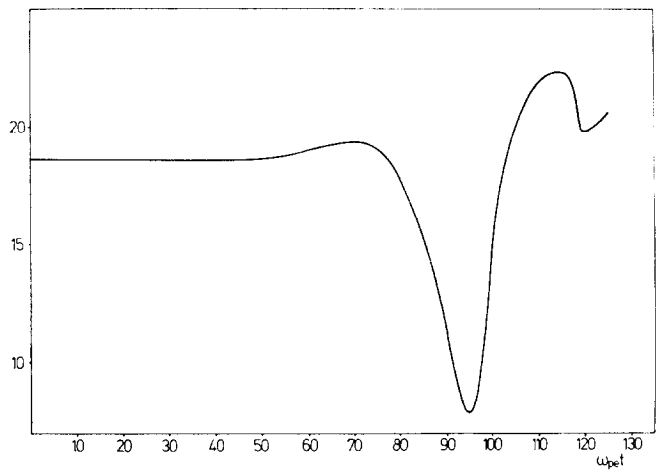

FIG. 8. Plasmon number PN (Eq. 17) as a function of time in units of $n_0 \kappa T_e / 2\omega_{pe}$.

APPENDIX: FLOW DIAGRAM

Initialization

(a) Initial values ($t = 0$) for

$$\rho,\ \varphi,\ E^{\text{hom}},\ v^{\text{hom}},\ x_\mu;\ v_\mu\ (t = -\Delta t/2);$$

(b) Beam density ρ_b ($t = 0$);

(c) Total electric field E ($t = 0$);

(d) New particle coordinates

$$x_\mu\ (t = \Delta t), \qquad v_\mu\ (t = \Delta t/2); \qquad v_\mu\ (t = 0);$$

(e) Initial mean beam current $-(e/m)(\rho_b v_b)^{\text{hom}}\,(t = 0)$;

(f) Second starting values $(t = -\Delta t)$ for

$$\rho,\ \varphi; \qquad E^{\text{hom}}\,(t = -\Delta t/2); \qquad \text{then put } t = 0.$$

Main Loop

(a) New background quantities:

$$\rho(t + \Delta t), \quad \varphi(t + \Delta t), \quad E^{\text{hom}}\left(t + \frac{\Delta t}{2}\right); \quad E^{\text{hom}}(t + \Delta t), \quad t^{\text{hom}}(t + \Delta t);$$

(b) New beam density $\rho_b\,(t + \Delta t)$;

(c) New electric field $E\,(t + \Delta t)$;

(d) New particle coordinates

$$x_\mu\,(t + 2\Delta t),\ v_\mu\,(t + \tfrac{3}{2}\,\Delta t),\ v_\mu\,(t + \Delta t)$$

(e) New mean beam current $-(e/m)(\rho_b v_b)^{\text{hom}}\,(t + \Delta t)$;

(f) $t \to t + \Delta t$.

ACKNOWLEDGMENT

We would like to thank Dr. H. Schamel for stimulating discussions.

REFERENCES

1. F. H. HARLOW, *in* "Methods in Computational Physics" (B. Alder, S. Fernbach, and M. Rotenberg, Eds.), Vol. 3, p. 319, Academic Press, New York, 1964.
2. B. M. MARDER, *Math. Comput.* **29** (1975), 434.
3. R. L. MORSE *et al.*, Papers D 113–116, 7th Am. Conf. on Plasma Simulation, 1975.
4. J. N. LEBŒUF, T. TAJIMA, AND J. M. DAWSON, UCLA-Report PPG-315, 1977.
5. R. L. MORSE, *in* "Methods in Computational Physics (B. Alder, S. Fernbach, and M. Rotenberg, Eds.), Vol. 9, p. 213, Academic Press, New York, 1970.
6. C. E. RATHMANN, J. L. VOMVORIDIS, AND J. DENAVIT, *J. Comput. Phys.* **26** (1978), 408.
7. L. E. THODE AND R. N. SUDAN, *Phys. Fluids* **18** (1975), 1552.
8. B. B. GODFREY, W. R. SHANAHAN, AND L. E. THODE, *Phys. Fluids* **18** (1975), 346.
9. A. CLEBSCH, *J. Reine Angew. Math.* **56** (1859), 1.
10. H. SCHAMEL AND K. ELSÄSSER, *J. Comput. Phys.* **22** (1976), 501.
11. C. K. BIRDSALL, A. B. LANGDON, AND H. OKUDA, *in* "Methods in Computational Physics" (B. Alder, S. Fernbach, and M. Rotenberg, Eds.), Vol. 9, p. 241, Academic Press, New York, 1970.
12. D. POTTER, "Computational Physics," Wiley, New York, 1973.
13. S. KAINER, J. M. DAWSON, R. SHANNY, AND T. P. COFFEY, *Phys. Fluids* **15** (1972), 493.

14. T. M. O'NEIL, J. H. WINFREY, AND J. H. MALMBERG, *Phys. Fluids* **14** (1971), 1204.
15. N. G. MATSIBORKO, I. N. ONISHCHENKO, V. D. SHAPIRO, AND V. I. SHEVCHENKO, *Plasma Phys.* **14** (1972), 591.
16. H. SCHAMEL, Y. C. LEE, AND G. J. MORALES, *Phys. Fluids* **19** (1976), 849.
17. K. ELSÄSSER AND H. SCHAMEL, *J. Plasma Phys.* **15** (1976), 409.
18. W. MAASJOST, Diplomarbeit, Bochum, 1977.